therapeutics

MDPI

Systematic Review

Systematic Literature Review of Epaxial Paraspinal Schwannomas: Differential Diagnosis and Treatment Approaches

Wassim Khalil [1,*,†], Roula Khalil [2,*,†], Alexandre Meynard [1], Alexandre Perani [3], Elodie Chaudruc [1], Mathilde Duchesne [3], Karine Durand [3], François Caire [1,4] and Henri Salle [1,5]

1 Department of Neurosurgery, Limoges University Medical Center, 87000 Limoges, France
2 UMR Inserm 1016, Institut Cochin, 75014 Paris, France
3 Department of Pathology, Limoges University Medical Center, 87000 Limoges, France
4 XLIM UMR CNRS 7252, Limoges University, 87000 Limoges, France
5 UMR Inserm 1308, CAPTuR "Contrôle de L'Activation Cellulaire, Progression Tumorale Et Résistance Thérapeutique", Faculty of Medicine, Limoges University, 87000 Limoges, France
* Correspondence: wassim.khalil@chu-limoges.fr (W.K.); roula.khalil@inserm.fr (R.K.)
† These authors contributed equally to this work.

Abstract: Background: Schwannomas, predominantly benign nerve sheath tumors, are typically found within the intradural extramedullary space of the spinal cord with potential extradural expansion. Other typical localizations are the upper limbs and neck area. Pure epaxial paraspinal schwannomas are very rare, often asymptomatic, and predominantly occur in the thoracic region, with only a handful of cases reported globally. The range of differential diagnoses for paraspinal lesions is extensive, emphasizing the importance of accurate diagnosis to ensure optimal therapy and avoid unnecessary treatments. **Method:** We conducted a systematic literature review searching for published recommendations for paraspinal lesion management in addition to examining the case of a 49-year-old male patient who presented with a history of persistent back pain. A thorough medical history and physical examination were followed by ultrasound and MRI, revealing a well-defined paravertebral mass spanning from T7 to T9. A secure ultrasound-guided biopsy was performed, leading to a preliminary diagnosis of paraspinal schwannoma. Subsequently, complete surgical resection was performed. **Results:** pathological reports confirmed the initial diagnosis of paraspinal schwannoma. Further investigation using FMI and RNA sequencing did not detect any specific genetic anomalies aside from an NF2 gene mutation. A follow-up MRI conducted six months later showed no signs of recurrence. **Conclusions:** The broad spectrum of differential diagnoses for paraspinal lesions necessitates a multidisciplinary approach to ensure accurate diagnosis and tailored treatment. This approach involves meticulous imaging interpretation followed by a secure biopsy procedure to obtain preliminary pathology results, ultimately leading to the implementation of the most suitable surgical treatment.

Keywords: Antoni A; Antoni B; dorsal ramus; epaxial lesion; nerve sheath tumor; paraspinal schwannoma; schwannoma

check for updates

Citation: Khalil, W.; Khalil, R.; Meynard, A.; Perani, A.; Chaudruc, E.; Duchesne, M.; Durand, K.; Caire, F.; Salle, H. Systematic Literature Review of Epaxial Paraspinal Schwannomas: Differential Diagnosis and Treatment Approaches. *Therapeutics* **2024**, *1*, 106–123. https://doi.org/10.3390/therapeutics1020010

Academic Editors: Dimitrios Tzachanis and Andrea Visentin

Received: 3 July 2024
Revised: 21 August 2024
Accepted: 4 December 2024
Published: 14 December 2024

Copyright: © 2024 by the authors. Licensee MDPI, Basel, Switzerland. This article is an open access article distributed under the terms and conditions of the Creative Commons Attribution (CC BY) license (https://creativecommons.org/licenses/by/4.0/).

1. Introduction

Tumors occurring in the paraspinal region represent a real challenge, owing to the complex interplay of various anatomical structures in this area. This region, characterized by its intriguing anatomy and proximity to critical spinal components, poses significant challenges in accurately diagnosing and managing its lesions [1]. From parietal fascia to paraspinal muscle aponeurosis, the paraspinal region serves as a base for the development of various tumors, originating either from the spine itself or the adjacent soft tissues. This intricate relationship underscores the necessity for a careful understanding of paraspinal

anatomy and radiological interpretation to effectively provide diagnostic and therapeutic options. Despite its clinical significance, few articles in the literature deal with lesions of the paraspinal region. Hence, this motivated us to realize a systematic literature review searching for current recommendations dealing with epaxial paraspinal lesions. Anatomically, the paraspinal region communicates with adjacent compartments such as the extradural neural axis, intercostal spaces, posterior mediastinum, pleura, and retroperitoneum, thus facilitating various modes of tumor spread [1]. These complex anatomical relationships not only increase the challenges in achieving complete tumor resection but also highlight the necessity for advanced radiological expertise for better preoperative planning [1].

Muscles form the major components of the paraspinal region. They are classified as either ventral hypaxial or dorsal epaxial muscle groups. Furthermore, due to their elongated nature spanning multiple spinal segments, pathological conditions affecting paraspinal muscles frequently propagate vertically along muscle fibers and fascial planes. This allows for tumor development over several segments. Numerous aponeuroses and fibrous fasciae cover the posterior surface of the epaxial region, posterior to the transverse and spinous processes. This explains the increased frequency of fibroblastic lesions in this area [2]. In addition, these fibrous layers restrict the inward spread of superficial soft-tissue tumors. However, the parietal fascia, composed of thin layers of connective tissue and covering the ventral side of the hypaxial region, does not impede tumorous invasion into adjacent pleura, posterior mediastinum, or retroperitoneum [3].

Spinal nerves emerge bilaterally through the intervertebral foramen between adjacent vertebrae. Upon its emergence, the spinal nerve bifurcates into two primary branches, namely the dorsal ramus and the ventral ramus. The dorsal ramus extends horizontally backward between the transverse processes to serve the epaxial region, encompassing the skin, epaxial muscles, and fasciae. In contrast, the ventral ramus exits the paraspinal region, potentially receiving connections from nearby sympathetic ganglia through rami communicantes before innervating the anterior trunk and limbs via a complex network of interconnecting nerves known as the plexus [1]. Radiologists play a crucial role in describing potential extensions into neural structures due to perineural spread, as this impacts the functional prognosis both before and after treatment, given the complex nerve anatomy complicating complete tumor excision [4].

The paravertebral space contains adipose tissues distributed between the muscles of the paraspinal area and along the nerves and vessels of the area. This space serves as a pathway for the extension of paraspinal lesions and is connected to the epidural space at the level of the intervertebral foramen [4,5].

Many lesions, both benign and malignant, can develop in the paraspinal area. Pure epaxial paraspinal schwannomas, considered among the rarest lesions in this area, grow between the paraspinal muscles. Only a limited number of case reports have been documented globally. Schwannomas are benign, solitary, slow-growing nerve sheath tumors [6,7]. They are the most common intradural extramedullary lesions of the spine, typically found in the epidural space of the thoracic area, followed by the lumbar and cervical regions. On the other hand, the paraspinal extension of schwannomas is extremely rare. Schwannomas exhibit a slight female predominance and occur most frequently between the ages of 40 and 50 years [7]. Several genetic diseases, including neurofibromatosis (especially type II) and Carney complex, have been associated with schwannomas [5]. Typically arising from a single fascicle, spinal schwannomas can expand from the epidural space through the intervertebral foramina into the extradural space, creating a dumbbell appearance on imaging. Symptoms associated with schwannomas depend on the localization and size of the lesion.

The muscular groups constituting the erector spinae are primarily innervated by the dorsal ramus of the spinal nerve. Paraspinal schwannomas, unlike their epidural counterparts, mainly arise from the dorsal ramus nerve and are typically asymptomatic. Notably, 80% of thoracic intramuscular schwannomas are asymptomatic compared to those affecting the upper limbs. Only seven cases of paraspinal dorsal root schwannomas

have been reported in the literature, with no molecular studies or clear guidelines for the appropriate management of affected patients. In the following article, we will deal with this issue. The patient's informed consent has been acquired.

2. Methods

2.1. Part 1: Literature Review

2.1.1. Search Objective

The objective of this review was to identify published consensus on the management of epaxial paraspinal schwannomas in order to provide clear guidelines for physicians to support their patients and administer appropriate treatment while minimizing unnecessary complications.

2.1.2. Search Criteria

The medical subject headings (MeSH) relevant to schwannomas include neurilemoma, neurinoma, schwannoma, schwannomatosis, and plexiform. We utilized these MeSH headings and terms to query the Cochrane Database of Systematic Reviews and the US National Library of Medicine (PubMed/MEDLINE). Below, we outline the structure of the literature queries conducted to explore relevant published articles on paraspinal schwannomas in these databases.

2.1.3. Search Keywords

- PubMed/MEDLINE was searched using the following query: (Schwannoma[Mesh]) AND (Spine[Majr]).
- The Cochrane database used the following:
  1. MeSH descriptor: [Spine] explode all trees.
  2. (paraspinal NEXT (lesion* or mass)) OR (epaxial NEXT (lesion* or mass)) OR (spinal NEXT (lesion* or mass)) OR ((paraspinal or epaxial) NEXT muscles).
  3. MeSH descriptor: [Schwannoma] explode all trees.
  4. (schwannoma) OR ("schwannomatosis") OR ("schwannomatoses").
  5. (#1 OR #2) AND (#3 OR #4).

Screening was then performed concerning abstracts of articles identified through the previous search parameters (n = 366), spanning publication dates from 1949 to March 2024. Additionally, manual searches were conducted using Google Scholar, resulting in the discovery of 5 additional abstracts which were added to the dataset.

2.1.4. Search Strategy

The website "RAYYAN", utilizing artificial intelligence, was employed for screening the abstracts of articles by two independent blinded groups of two reviewers each to mitigate bias. The approved articles from the two reviewer groups were pooled, and out of the 371 articles screened, 53 were selected for full-text review following a rapid abstract screening, with inclusion criteria focused on schwannomatous lesions.

Subsequently, upon review by the two groups, 44 articles were excluded, as they focused on lesions within the spinal canal (intra/extradural), foraminal, retroperitoneal, mediastinal/retropleural, or anterior cervical spine (Figure 1). A table summarizing the remaining articles (n = 9) pertaining to epaxial paraspinal schwannomas published between 2014 and 2022 was then created (Table 1) [7–15], as this was focus of this literature review.

This systematic review was conducted in accordance with the PRISMA 2020 guidelines to ensure transparency and completeness in reporting. The systematic review was not registered on PROSPERO because the platform does not accept reviews that have already begun or completed data extraction. PROSPERO's purpose is to record information at the study's design stage.

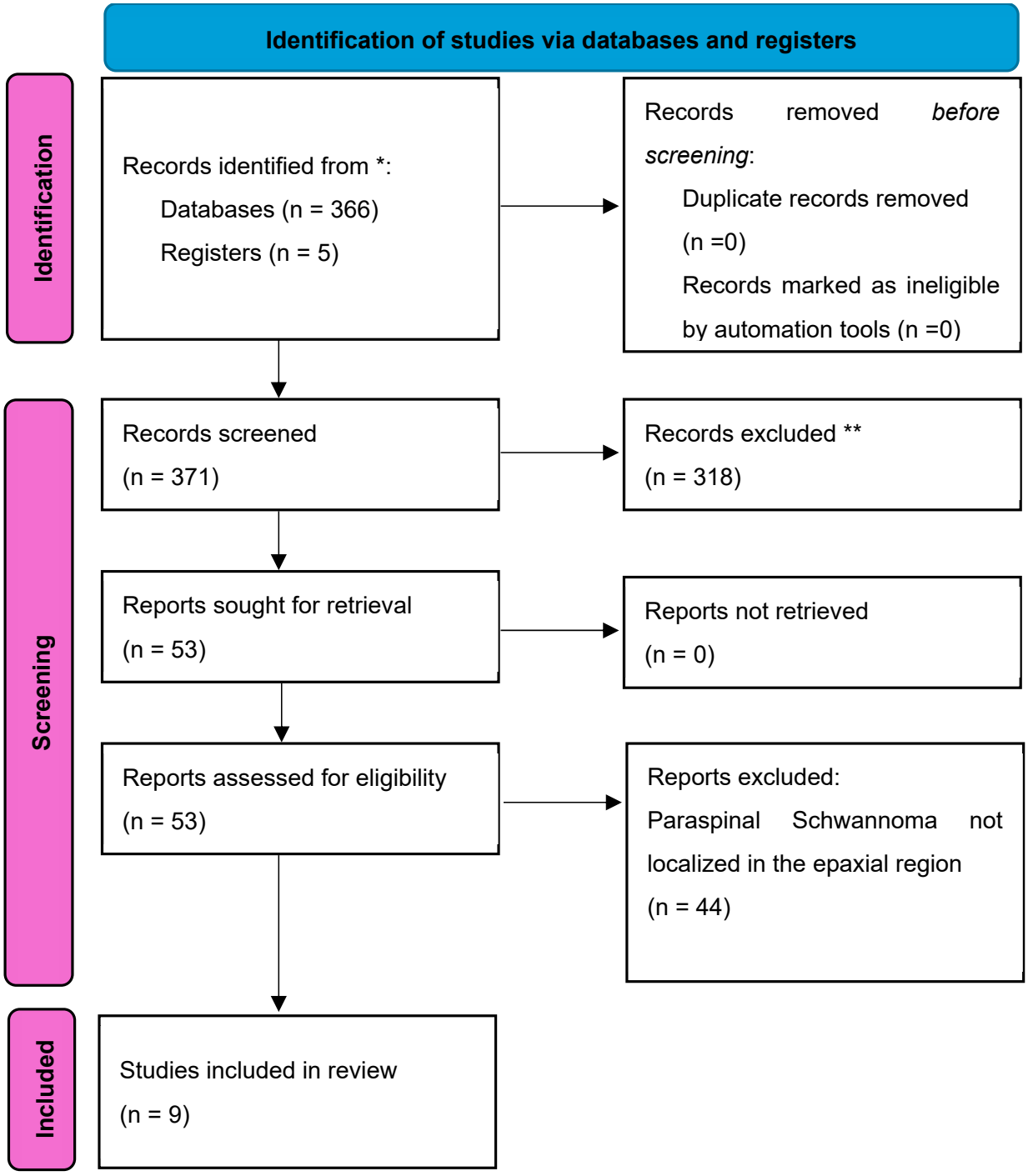

Figure 1. A PRISMA 2020 flow diagram illustrating the methodology used in the systematic literature review. * Screening is performed concerning abstracts of articles identified through the previous search parameters (n = 366), spanning publication dates from 1949 to March 2024. Additionally, manual searches are conducted using Google Scholar, resulting in the discovery of 5 additional abstracts. ** The website "RAYYAN", utilizing artificial intelligence, is employed for screening the abstracts of articles supervised by two independent blinded groups of two reviewers each to mitigate bias. The pooled approved abstracts from both teams are 53, with 318 rejected abstracts dealing with lesions other than schwannomas.

Table 1. Published cases of paraspinal schwannomas for the past 11 years. Table showing patients' sex, age, presenting symptoms, localization, imaging, and histological characteristics in addition to the realized treatment and recurrence after up to 1 year follow-up.

Publication	**Ohla V. et al. (2014) [8]**	**Kim JH et al. (2015) [10]**	**Shah KA et al. (2018) [12]**	**Kim D-G et al. (2019) [9]**	**Emengen A. et al. (2019) [13]**	**Keskin et al. (2020) [14]**	**Kim, Y.G et al. (2020) [11]**	**Pace, S. et al. (2021) [15]**	**Valsecchi et al. (2022) [7]**
Gender	Female	Female	Male	Male	Female	Female	Male	Female	Female
Age	34	62	45	39	47	32	79	15	69
Symptoms	Deep, dull, and diffuse lower back pain	Growing mass in the lumbar area with recent pain upon palpation	Asymptomatic slow-growing mid-thoracic paravertebral lesion	Upper back mass slowly growing and causing discomfort when lying down	Back pain, burning sensation	No symptoms, only growing mass in upper back	Right lower back tenderness	Lower back, upper buttock pain with underlying mass recurring for the third time	Right dorsal paravertebral numbness
Neurological deficit	No sensory or motor deficit	No sensory or motor deficit	No sensory or motor deficit	No sensory or motor deficit	No sensory or motor deficit	No sensory or motor deficit	No sensory or motor deficit	No sensory or motor deficit	No sensory or motor deficit
Localization	Lumbar region	Lumbar region	Thoracic region	Thoracic region	Cervical region	Thoracic region	Lumbar region	Lumbo-sacral region	Thoracic region
Level	L4-L5	L2-L4	T9-T11	T1-T4	C7-T1	T7-T8	L5-S1	L5-S5	T3-T5
Imaging findings	Well-defined ovoid lesion. Hypointense T1W. Heterogeneous enhancement	Well-defined lobulated lesion. Heterogeneous low signal intensity on T1 and high signal intensity on T2W. Heterogeneous enhancement	Fascicular bundle revealed by hypointense foci within hyperintense area on T2W	Heterogeneous T1 and T2W high signal intensity. Peripheral irregular heterogeneous contrast enhancement with central non-enhancement	Well-circumscribed lesion. Hyperintense T2W. Hypointense T1W. Peripheral contrast enhancement with necrotic center	Well-circumscribed lesion. Hyperintense periphery on T2W and hypointense in center. Hypointense T1W. Peripheral contrast enhancement with necrotic center	Well-circumscribed lesion. Hyperintense periphery on T2W with target signs, hypointense in center. Hypointense T1W. peripheral contrast enhancement with a necrotic center	Ultrasound superficial heterogenous soft-tissue mass (9.09 × 7.01 cm.). Large soft-tissue mass with hypervascularity on MRI. Multiple satellite lesions of varying dimensions on CT	Well-circumscribed lesion. Hypointense T1W. Hyperintense heterogenous cystic components on T2W. Peripheral contrast enhancement of solid component. Identified entry/exit nerve
Treatment	Total excision	Total excision	Total excision	Total excision	Preoperative biopsy followed by total excision	Total excision	Total excision	Total excision	Total excision
Pathology and immunohistochemistry results	Cellular Antoni A zones. Hypo-cellular Antoni B zones. Neuropathological staining is positive for S100 and Vimentin.	Compact spindle cell regions (Antoni A). Loosely arranged areas of lower cell density (Antoni B). Diffuse immunostaining with S-100 antibody.	Cellular Antoni A zones with Verocay bodies. Hypocellular Antoni B zones.	Antoni A-like arrangement in peripheral portion of lesion. Degenerative changes in central necrotic cavity. Diffuse immunostaining with S-100 antibody.	Cellular Antoni A zones with Verocay bodies. Hypocellular Antoni B zones.	Cellular Antoni zones. Hypo-cellular Antoni B zones. Diffuse immunostaining with S-100 antibody.	Cellular Antoni A zones. Hypo-cellular Antoni B zones. Diffuse immunostaining with S-100 antibody.	Nodules showed plexiform architecture with intact fibrous capsules. Variable cellular components, focal necrosis, scattered mitotic activity. Diffuse S-100 positivity and patchy Ki-67 moderate activity.	Hyalinized blood vessels. Partial loss of Antoni A areas with Verocay bodies. Cellular shape irregularity. Hyperchromatic nuclei. Thrombi formation.
Recurrence	No recurrence at 6-month follow-up	No follow-up mentioned	No recurrence at 6-month follow-up.	No recurrence at 12-month follow-up.	No recurrence at 8-month follow-up.	No recurrence at 4-month follow-up.	Unknown	5 weeks good local evolution, no control imaging realized	No recurrence at 12-month follow-up.
Study type	Case report	Case report	Case report	Case report	Case report	Case report	Case report	Case report	Case report
Source	Google Scholar	PubMed	PubMed	PubMed	Google Scholar	Google Scholar	Google Scholar	PubMed	Google Scholar

2.2. Part 2: Case Presentation

2.2.1. Case Presentation

A 49-year-old male with several years of history of back pain was admitted to our center following severe worsening of his pain. Upon physical examination, a firm mobile mass was detected in the upper back region, with tenderness upon palpation. There were no motor or sensory deficits. Subsequent ultrasound and MRI were realized, revealing a well-delineated ovoid paravertebral mass extending from T7 to T9, measuring 80 × 28.4 × 20 mm (Figure 2). The lesion exhibited a heterogeneous hypointense signal on T1-weighted imaging, a hyperintense signal on T2-weighted imaging, and diffuse contrast enhancement on T1+C (Figure 2). Given the broad differential diagnosis for paraspinal lesions and the limitations of relying solely on radiologic findings, an ultrasound-guided biopsy was conducted to obtain a definitive diagnosis. Pathological results confirmed the preliminary diagnosis of schwannoma, with positive S100 and SOX10 (SRY-related HMG-box 10) proteins.

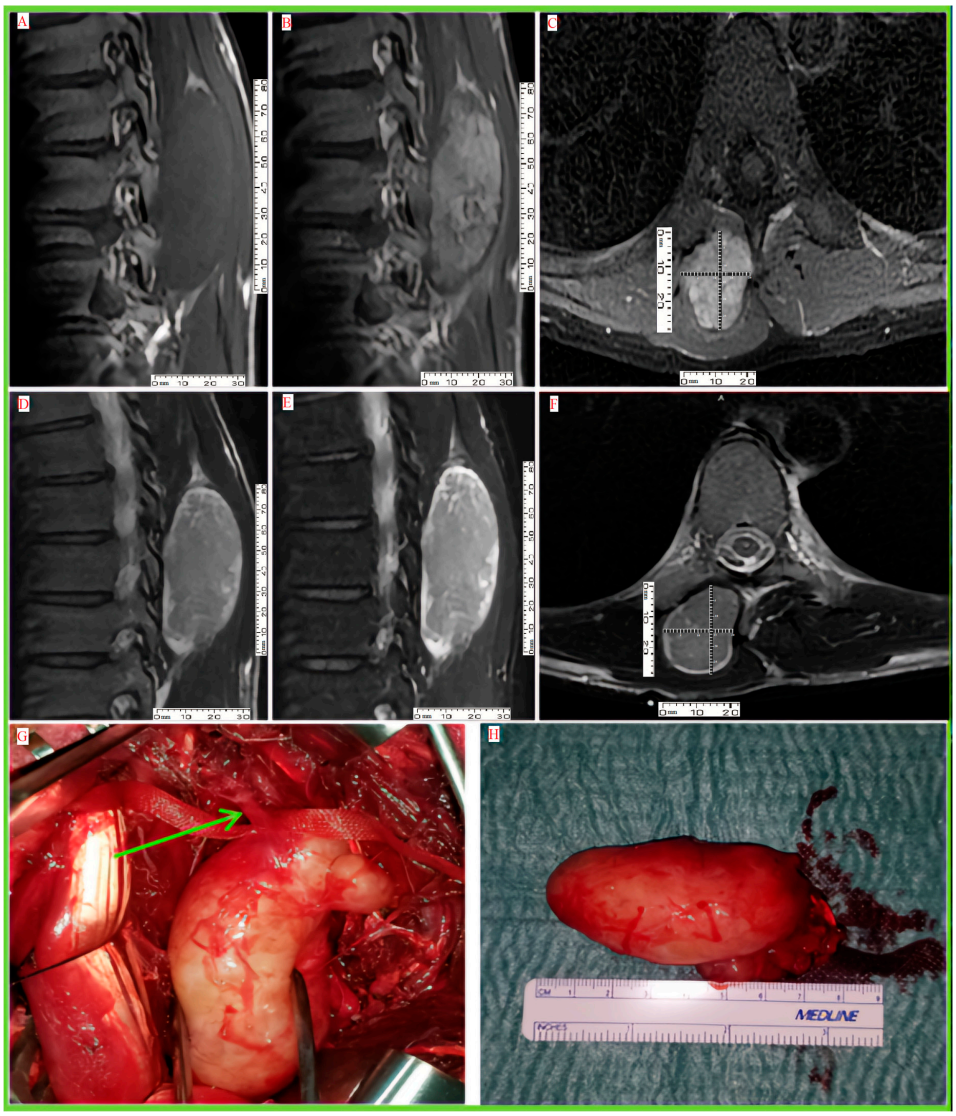

Figure 2. Preoperative MRI along with perioperative pictures. (**A**,**B**) Sagittal MRI showing well-defined hypointense lesion with post gadolinium diffuse enhancement. (**C**) T1 + contrast axial MRI. (**D**,**E**) Hyperintense T2W and T2 flair MRI, respectively. (**F**) T2W axial MRI. (**G**,**H**) Perioperative picture showing encapsulated schwannoma along with its rostral attachment to dorsal ramus (indicated by arrow).

2.2.2. Surgical Technique

The decision to perform a complete surgical excision was made. The procedure was realized under general anesthesia in a prone position. An ultrasound probe was used to precisely localize the lesion, then a paramedian incision was made. Blunt dissection was continued through the paravertebral muscles, and the encapsulated lesion was identified. Careful dissection was then performed, successfully revealing the dorsal nerve root situated on the uppermost side of the lesion. In toto excision was then performed after the coagulation and severing of the dorsal root nerve.

2.2.3. Performed Examinations on the Specimen
Pathology/Immunohistochemistry

The surgical specimen was sent to the pathology laboratory for analysis, comprising standard anatomopathological assessments and immunohistochemistry studies. The prepared slides were stained with hematoxylin phloxine saffron (HPS stain) and then examined by pathologists using optic microscopy. Furthermore, immunohistochemistry analysis was conducted using an anti-S100 protein antibody (Figure 3).

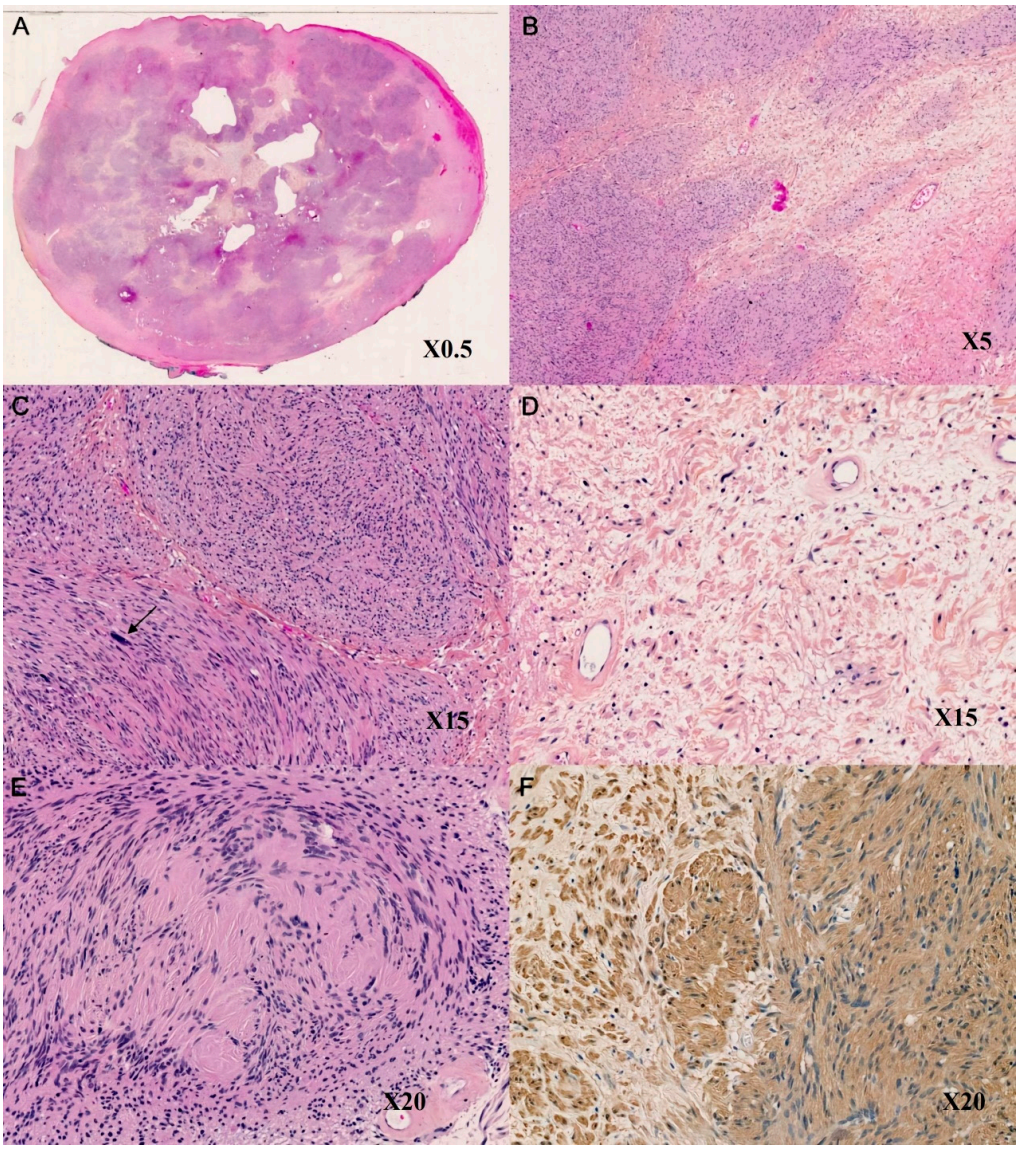

Figure 3. Pathological findings of the lesion. (**A**–**E**) Hematoxylin phloxine saffron stain, optic microscopy. (**F**) Immunohistochemistry analysis with an anti-S100 protein antibody, optic microscopy.

(**A**) The tumor is well circumscribed and finely encapsulated (×0.5 magnification). (**B**) The biphasic aspect of the tumor, composed of cellular and compact areas (Antoni A) on the left of the picture and loosely arranged areas (Antoni B) on the right of the picture (×5 magnification). (**C**) Antoni A areas showing a fasciculate arrangement, composed of tumoral Schwann cells with modest eosinophilic cytoplasm, with no discernible cell borders and with rounded or elongated nuclei associated with a nuclear pleomorphism and some bizarre appearing nuclei (arrow) (×15 magnification). (**D**) Antoni B areas composed of a few tumoral Schwann cells in a loose stroma (×15 magnification). (**E**) Verocay bodies consisting of tumoral Schwann cells with a palisading arrangement and aligned cell processes (×20 magnification). (**F**) Diffuse and homogenous staining with the S100 protein antibody (×20 magnification).

RNA Extraction

Further genetic analysis was conducted using RNA sequencing, also known as RNA-seq, using the following analysis method:

- Extraction technique using Maxwell® RSC RNA formalin-fixed paraffin-embedded tissue samples (FFPE) Kit—Promega without DNase (AS8500 RSC 48 application software, Madison, WI USA). This instrument provides an easy method for the efficient automated purification of RNA from mammalian FFPE tissue samples.
- Next-generation sequencing (NGS) method using a MiSeq Illumina high-throughput sequencer.
- Analysis using Archer Analysis 5.1.7 software.
- Targeted RNA-seq using Archer FusionPlex® Lung panel (ArcherDx), testing for ALK, BRAF, EGFR, ERBB2, FGFR1, FGFR2, FGFR3, FGFR4, KRAS, MET, NRG1, NTRK1, NTRK2, NTRK3, NUTM1, PIK3CA, RET, and ROS1.

  Analytical thresholds of the Archer Analysis 5.1.7 software included the following:
- Analytical sensitivity (20% of tumor cells): The analysis is sensitive enough to detect variations present in at least 20% of the tumor cells within the sample. In our case, 80% of our sample was composed of tumoral cells.
- Minimum reads (=1,000,000): This threshold specifies the minimum number of sequencing reads required for reliable analysis. In this case, for example, at least 1,000,000 sequencing reads were necessary to guarantee adequate coverage and depth for accurate variant calling and fusion detection.
- Average unique RNA start sites per control (GSP2 $\geq$ 10.0): This threshold refers to the average number of unique RNA start sites observed in control samples. An average value of 10.0 or higher shows robust coverage and sufficient sequencing depth in the control samples, guaranteeing a reliable comparison and analysis of the experimental data.
- RNA fragment size > 100 base pairs (bp): This threshold stipulates the minimum size of RNA fragments considered for analysis. Fragments smaller than 100 bp may not provide sufficient information for accurate sequencing and alignment; thus, they are excluded from the analysis.
- Significant fusion percentage reads > 10%: This threshold defines the minimum percentage of sequencing reads that can support a fusion event to be considered significant. Fusions with more than 10% of the total reads supporting them are considered significant and likely represent genuine fusion events rather than the background noise or artifacts.
- Significant single nucleotide polymorphism (SNP) variant allele frequency (VAF) > 5% and minimum depth 100×: This threshold specifies that SNPs with a VAF greater than 5% are considered significant. Additionally, a minimum sequencing depth of 100× (coverage of 100 reads or more) is required to ensure the reliability of SNP calls.

Genomic Analysis (FMI)

Genomic analysis was conducted using the FoundationOne®CDx, searching for individual genomic alteration affecting our patient. Of note is that this test, developed by "Foundation Medicine Inc. (FMI)", is the first FDA-approved tissue-based broad companion

diagnostic (CDx) for solid tumors, backed by rigorous clinical and analytical validations. FoundationOne® CDx offers crucial markers such as microsatellite instability (MSI) and tumor mutational burden (TMB) [16]. Formalin-fixed paraffin-embedded (FFPE) tumor samples were sent to Foundation Medicine Inc. (FMI) for comprehensive analysis. The FMI analysis involved the extraction of genomic DNA, followed by hybridization-based capture and sequencing of all coding exons of 309 genes, along with the intronic or non-coding regions of 21 genes and selected intronic or non-coding regions from an additional 15 genes, resulting in a total of 324 targeted genes.

Additionally, the test provided information on microsatellite instability (MSI), tumor mutational burden (TMB) status, and tumoral fraction. Data analysis utilized a customized pipeline designed to detect various genomic alterations, including base substitutions, nucleotide insertions and deletions (indels), copy number alterations (amplifications and homozygous gene deletions), and select genomic rearrangements (e.g., gene fusions). The main report contained known and likely pathogenic variants, along with suggestions for targeted therapeutics. Subsequently, the results were received and reviewed by the biologists at the Cancer Molecular Genetics Platform (Plateforme de Génétique Moléculaire des Cancers—PGMC) at Limoges University Hospital, an accredited platform by the National Institute of Cancer, France.

In addition to a supplementary data report of all variants, including variants of unknown significance (VUSs), variants classified as VUSs were further examined by biologists of the platform and reclassified based on a review of international variant classification databases (ClinVar, dbSNP, GnomAD, COSMIC, LOVD, Varsome, OncoKB™, or Mobidetails site) [17], as well as in silico analyses using tools such as SPIP and Splice-AI for splice site alteration prediction, and SIFT, Polyphen, FATHMM, AlphaMissense, REVEM, ClinPred, and CADD for predicting the impact of gene alterations on pathogenicity and protein function [18].

3. Results

3.1. Pathology/Immunohistochemistry

Pathological analysis revealed a well-defined biphasic lesion comprising typical alternating compact Antoni A areas and loosely arranged Antoni B areas surrounded by a fibrous capsule. The tumoral cells exhibited pronounced nuclear pleomorphism with scattered nuclei showing atypical-to-bizarre appearances. Verocay bodies were also noted, with minimal mitotic activity observed and no evidence of necrosis. The immunohistochemical tests revealed diffuse and homogeneous S100 protein expression throughout the tumor cells. Neurofilament staining was negative, and a mild expression of epithelial membrane antigens was detected in a few scattered perineurial cells within the capsule but not within the tumor. Findings were suggestive of a schwannoma, classified as Grade 1 according to the WHO classification.

3.2. RNA Extraction

Further genetic analysis was performed using RNA sequencing (RNA-seq), a technique that assesses the expression levels of active genes in a biological sample. This method provides insights into gene regulation, cellular responses to stimuli, mutation detection, and novel transcripts. The heatmap of RNA-seq (Figure 4) illustrates the relative gene expression profile of our patient, analyzed alongside 13 other tumor samples using the same RNA-seq technique. The patient's data are highlighted in red boxes on the heatmap. For normalization, we used the CHMP2A, GPI, RAB7A, and VCP genes, which encode ubiquitously expressed proteins. Relative expression values are presented as log2 ratios, comparing gene expression to normalization genes. These values are depicted on a color scale from -6 (indicating loss of expression) to 6 (indicating overexpression), with 0 representing normal expression levels. No significant overexpression, loss of expression, fusion transcripts, or other transcriptome abnormalities, such as alternative splicing variants or

amplifications, were detected. Additionally, no point mutations were identified in the analyzed genes.

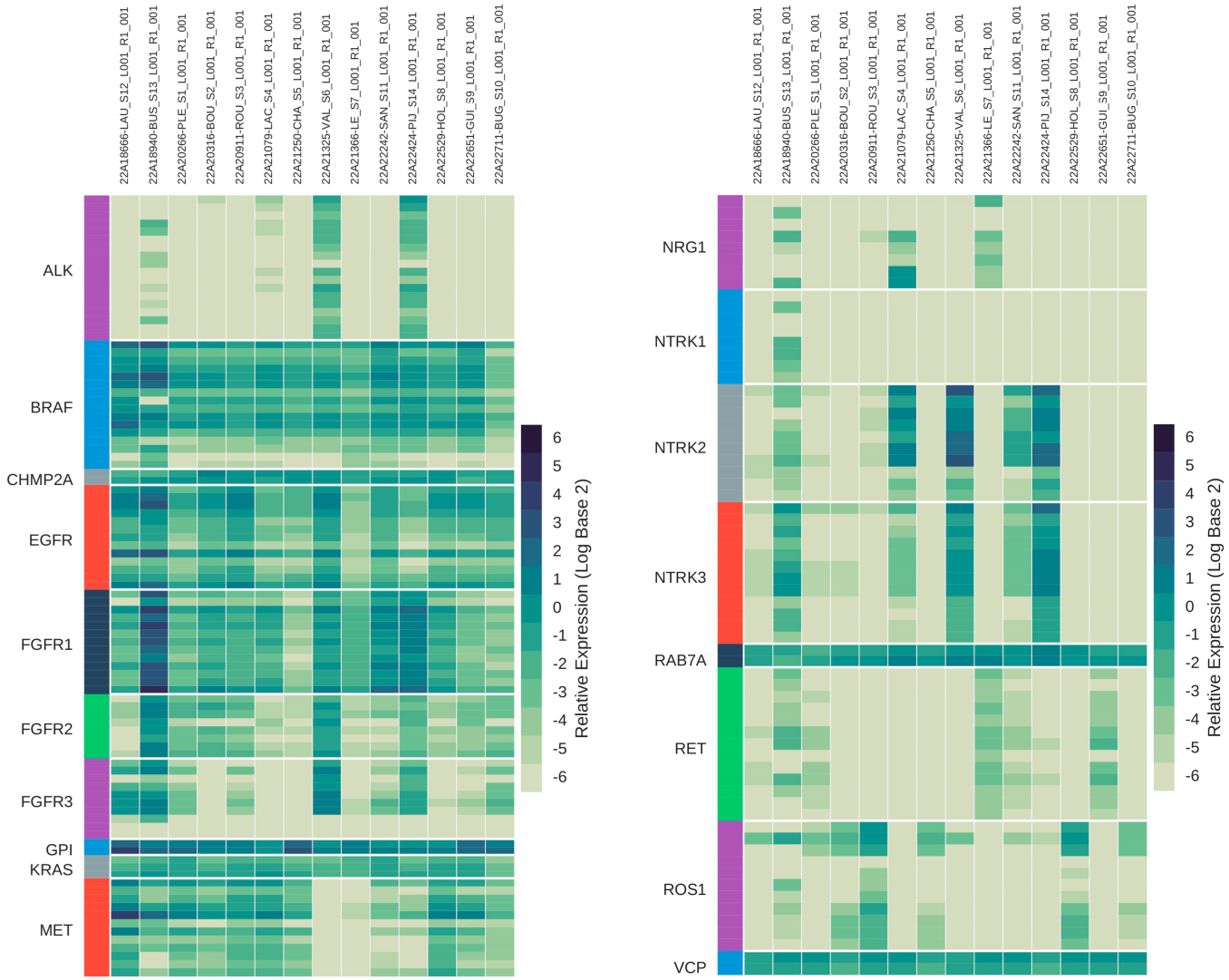

Figure 4. Relative gene expression profile in paraspinal schwannoma (our patient's data were highlighted in red). Log^2 ratios of expression are normalized using CHMP2A, GPI, RAB7A, and VCP genes, shown on a color scale from −6 (loss) to 6 (overexpression), with 0 representing normal expression levels.

3.3. Genomic Analysis (FMI)

Genomic analysis was conducted using the FoundationOne®CDx, searching for individual genomic alteration affecting our patient. The test was positive for a genetic alteration affecting the NF2 gene located on chromosome 22, characterized by the loss of exon 1, in addition to the detection of a few variants of unknown significance by this test, revealed after reclassification by biologists of the PGMC platform (Table 2). The impact of those variants is currently unknown.

Following this extensive testing and analysis, no fusion transcripts or other transcriptome anomalies (such as alternative intron splicing variants or amplifications) were detected within the scope of the utilized panel and the sensitivity of the employed techniques. Further investigations and alternative diagnostic approaches are necessary to reveal unique molecular characteristics of paraspinal intramuscular schwannomas.

Table 2. Large-panel genomic analysis using the FoundationOne®CDx test. This table regroups all variants classified as VUSs by the FMI as variants of unknown significance (VUSs). Significance was then re-examined by the biologists of the Cancer Molecular Genetics Platform of Limoges University Medical Center.

Gene	Reference	Conical	Nucleotide Alteration	Human Genome Variation Society (HGVS)	Effect	Variation in Allelic Frequency	Variant Classification (FMI)	Variant Classification (Local)	Concordance FMI/ Local Classification	Comments
BRCA1	NM_007294	Yes	4358-552C>TT	c.4358-552delinsTT:p.	non-coding	0.94%	VUS (class 3)	NA (artifact?)	No	Insertion in low-complexity region
BRCA1	NM_007294	Yes	4358-552C>T	c.4358-552C>T:p.(?)	non-coding	43.05%	VUS (class 3)	Likely benign (Class 2)	No	Substitution in low-complexity region 1 homozygous carrier in GnomAD
BRCA1	NM_007294	Yes	4358-552deIC	c.4358-552del:p.(?)	non-coding	1.30%	VUS (class 3)	NA (artifact?)	No	Low-complexity region. Guanin deletion in 5 of 2 guanins
CUL4A	NM_003589	NM_001008895.4	69-81G>A	c.69-81G>A:	non-coding	48.75%	VUS (class 3)	Likely benign (Class 2)	No	Oncogenic mechanism = gain of function (OncoKB). Heterozygous carriers in GnomAD; no splice effect (SPiP). Located in AluSx3 sequence
CUL4A	NM_001008895.4	Yes	c.369-81G>A	c.369-81G>A:p.(?)	non-coding	48.75%		Likely benign (Class 2)	No	Oncogenic mechanism = gain of function (OncoKB). Heterozygous carriers in GnomAD; no splice effect (SPIP). Located in AluSx3 sequence
PIK3C2B	NM 002646	NM_001377334.1	2678+2T>G	c.2678+2T>G:p.(?)	splice site	0.62%	VUS (class 3)	Likely benign (Class 2)	No	Mechanism = gain of function (OncoKB). Upstream of functional sites (UniProt). Splice alteration predicted two heterozygous carriers in GnomAD
PIK3C2B	NM_001377334.	Yes	c.2678+2T>G	c.2678+2T>G	splice site	0.62%		Likely benign (Class 2)	No	Mechanism = gain of function (OncoKB). Upstream of functionnal sites (UniProt). Splice alteration predicted two heterozygous carriers in GnomAD
POLD1	NM_002691	Yes	2103C>T	c.2103C>T p.(Tyr701=)	synonymous	48.57%	VUS (class 3)	Likely benign (Class 2)	No	Silent mutation, no splice effect (SPiP). Heterozygous carriers in GnomAD; out-of-exonuclease domain; likely benign/benign (ClinVar/LOVD)
BRAF	NM_004333	Yes	981-2434C>T	c.981-2434C>T:p.(?)	non-coding	48.71%	VUS (class 3)	Likely benign (Class 2)	No	Mechanism = gain of function (OncoKB). Heterozygous carriers in GnomAD; possible mismapping (GRCh37:chr18:g36680345 36,680,364 FHOD3 intron 14)
PDK1	NM_002610	Yes	840T>G	c.840T>G:p.(Leu280=)	synonymous	51.12%	VUS (class 3)	Likely benign (Class 2)	No	Mechanism gain of function (OncoKB). Located in kinase domain >100 heterozygous carriers in GnomAD; no splice effect (SPIP)
ERRFI1	NM_018948	Yes	126-20G>A	c.126-20G>A:p.(?)	non-coding	51.35%	VUS (class 3)	Likely benign (Class 2)	No	Mechanism loss of function (OncoKB). Poorly conservated, no splice alteration, heterozygous carriers in GnomAD
ERBB3	NM_001982	Yes	1184-23T>C	c.1184-23T>C:p.(?)	non-coding	51.13%	VUS (class 3)	Likely benign (Class 2)	No	Mechanism = gain of function (OncoKB). Splice alteration risk = 98% (SPIP)
MERTK	NM_006343	Yes	845-15_845-14insGTGTGTGTGT	c.845-15_845-14insGTGTGTGTGT:p.(?)	non-coding	0.97%	VUS (class 3)	Likely benign (Class 2)	No	Microstaellite simple tandem repeat (TG)
MERTK	NM_006343	Yes	845-15_845-14insGTGTGTGT	c.845-15_845-14insGTGTGTGT:p.(?)	non-coding	42.79%	VUS (class 3)	Likely benign (Class 2)	No	Microstaellite simple tandem repeat (TG)
CEBPA	NM_004364	Yes	557_558insACC	c.557_558insACC:p(Pro189dup)	inframe insertion	0.76%	VUS (class 3)	Likely benign (Class 2)	No	Mechanism loss of function; low-complexity region repetition of seven proline (Pro183_Pro189). Heterozygous carriers in GnomAD. Unknown in OncoKB
ATR	NM_001184	Yes	5898+45_5898+82del38	c.5898+45_5898+82del:p.(?)	non-coding	59.65%	VUS (class 3)	Benign (Class 1)	No	Microsatellite (simple tandem repeat TA(29)). Homozygous carriers in GnomAD
ATR	NM_001184	Yes	5898+47_5898+82del36	c.5898+47_5898+82del:p.(?)	non-coding	29.17%	VUS (class 3)	Benign (Class 1)	No	Microsatellite (simple tandem repeat TA(29). Homozygous carriers in GnomAD

Table 2. *Cont.*

Gene	Reference	Conical	Nucleotide Alteration	Human Genome Variation Society (HGVS)	Effect	Variation in Allelic Frequency	Variant Classification (FMI)	Variant Classification (Local)	Concordance FMI/ Local Classification	Comments
RUNX1	NM_001754	Yes	1264G>A	c.1264G>A:p.(Glu422Lys)	missense	2.27%	VUS (class 3)	VSI (class 3)	Yes	Mechanism loss of function (OncoKB). Others missenes (Asp/Gly/Val/Ala/Gin) in GnomAD. Unknown OncoKB, VUS ClinVar. Conflicting in silico predictions
FGF12	NM 021032	NM_004113.6	415-8 415-7TC>CTT	c.415-8_415-7delinsCTT:1	non-coding	1.47%	VUS (class 3)	VSI (class 3)	Yes	Unknown oncogenic mechanism (majority of gain of function for others' isotypes). Unknown OncoKB. Located three low-complexity regions A(13). Poorly conservated region. Exon 4/5
FGF12	NM_004113.6	Yes	c.229-8 229-7delinsCTT	c.229-8_229-7delinsCTT:p.(?)	non-coding	1.47%		VSI (class 3)	Yes	Unknown oncogenic mechanism (majority of gain of function for others' isotypes). Unoknown OncoKB. Located three low-complexity regions A(13). Poorly conservated region. Exon 5/6 on this transcript
FGF12	NM_021032	NM_004113.6	415-9 415-7TTC>CTT	c.415-9_415-7delinsCTT:p.(?)	non-coding	37.76%	VUS (class 3)	VSI (class 3)	Yes	Unknown oncogenic mechanism (majority of gain of function for others' isotypes). Unknown OncoKB. Located three low-complexity regions A(13). Poorly conservated region. Exon 4/5
FGF12	NM_004113.6	Yes	c.229-9_229-7delinsCTT	c.229-9_229-7delinsCTT:p.(?)	non-coding	37.76%	-	VSI (class 3)	Yes	Unknown oncogenic mechanism (majority of gain of function for others' isotypes) Unknown OncoKB. Located three low-complexity regions A(13). Poorly conservated region. Exon 5/6 on this transcript
FGF12	NM 021032	NM_004113.6	415-10 415-7TTTC>CTT	c.415-10_415-7delinsCTT:p.(?)	non-coding	4.57%	VUS (class 3)	VSI (class 3)	Yes	Unknown oncogenic mechanism (majority of gain of function for others' isotypes). Unknown OncoKB. Located three low-complexity regions A(13) Poorly conservated region. Exon 4/5
FGF12	NM_004113.6	Yes	c.229-10_229-7delinsCTT	c.229-10_229-7delinsCTT:p	non-coding	4.57%		VSI (class 3)	Yes	Unknown oncogenic mechanism (majority of gain of function for others' isotypes). Unknown OncoKB. Located three low-complexity regions A(13). Poorly conservated region. Exon 5/6 on this transcript
PALB2	NM_024675	Yes	3073G>A	c.3073G>A:p.(Ala1025Thr)	missense	50.67%	VUS (class 3)	Likely benign (Class 2)	No	>20 heterozygous carriers in GnomAD
RARA	NM 000964	Yes	179-2541C>A	c.179-2541C>A:p.(?)	non-coding	50.28%	VUS (class 3)	Likely benign (Class 2)	No	Mechanism = fusions (OncoKB). Deep intronic located in simple tandem repeat
EGFR	NM 005228	Yes	1880+2154_1880+ 2155insATGGTGG TGGTGTTGATG	c.1880+2154 1880+ 2155insATGGTGGTG	non-coding	69.06%	VUS (class 3)	VSI (class 3)	Yes	Probably corresponds to insertion of intron EGFR intron 1 sequence (chr7:chr7:55167218 55,167,591 (identities 362/374(97%) gap 9/374(2%))
EPHA3	NM 005233	Yes	930C>T	c.930C>T:p.(Tyr310=)	synonymous	0.64%	VUS (class 3)	Likely benign (Class 2)	No	Mechanism loss of funtion. Silent mutation; no splice effect (SPIP). Heterozygous carriers in GnomAD
SMARCB1	NM 003073	Yes	645T>G	45T>G:p.(Pro215=)	synonymous	0.97%	VUS (class 3)	Likely benign (Class 2)	No	Mechanism loss of function (OncoKB). Likely benign ClinVar; no splice effect (SPIP). Heterozygous carriers in GnomAD
ALK	NM 004304	Yes	2257C>T	c.2257C>T:p.(Arg753Trp)	missense	0.68%	VUS (class 3)	Likely benign (Class 2)	No	Poorly conservated. Unknown OncoKB. Out-of-tyrosin kinase domain
NTRK3	NM 001007156	NM_001012338.3	1721-18delT	c.1721-18del:p.	non-coding	1.64%	VUS (class 3)	Likely benign (Class 2)	No	Mechanism = gain of function. Heterozygous carriers in GnomAD. No splice effect (SPIP)
NTRK3	NM_001012338.3	Yes	c.1586-38728del	c.1586-38728del:p.(?)	non-coding	1.64%		Likely benign (Class 2)	No	Low-complexity region. Deep intronic. Heterozygous carriers in GnomAD

Table 2. *Cont.*

Gene	Reference	Conical	Nucleotide Alteration	Human Genome Variation Society (HGVS)	Effect	Variation in Allelic Frequency	Variant Classification (FMI)	Variant Classification (Local)	Concordance FMI/ Local Classification	Comments
SMARCA4	NM_003072	Yes	3168+13C>T	c.3168+13C>T:	non-coding	49.87%	VUS (class 3)	Likely benign (Class 2)	No	Mechanism = gain of function (OncoKB). No splice effect (SPIP). Heterozygous carriers in GnomAD
NBN	NM_002485	Yes	511A>G	c.511A>G:p.(Ile171Val)	missense	47.93%	VUS (class 3)	Benign (Class 1)	No	Mechanism loss of function. Homozygous carriers in GnomAD (autosomic recessive disease)
RAF1	NM_002880	Yes	680+950_680+951insCATA	c.680+950_680+951insCATA	non-coding	36.61%	VUS (class 3)	Benign (Class 1)	No	Insertion in low-complexity region TG(16). Heterozygous carriers in GnomAD
FANCG	NM_004629	Yes	1207G>A	c.1207G>A:p.(Ala403Thr)	missense	51.48%	VUS (class 3)	VSI (class 3)	Yes	Mechanism loss of function. Unknown LOVD. No homozygous carriers in GnomAD (autosomic recessive disease). In silico mainly pathogenic
RAD52	NM 134424	Yes	348+60G>A		non-coding	48.73%	VUS (class 3)	Benign (Class 1)	No	Not involved in cancer disease, not OMIM. Morbid gene. Heterozygous carriers in GnomAD
FGFR1	NM_023110	Yes	189+1075-89+1086TGGG GGGGGGGT>GGGGG	c.-89+1075_-89+1086delinsGGGGG:p	5′UTR variant	2.57%	VUS (class 3)	Likely benign (Class 2)	No	Low-complexity region (CAC repeat). Multiple different alleles in GnomAD
ARID1A	NM_006015	Yes	4005-42G>A	4005-42G>A	non-coding	10.46%	VUS (class 3)	Benign (Class 1)	No	>40 heterozygous carriers in GnomAD

4. Discussion

Paraspinal schwannomas are rare encapsulated tumors located in the paraspinal area, with few documented reports of pure epaxial localization worldwide (Table 1). A review of reported cases reveals a prevalence among females, with an average age range consistent with the existing literature (40–70 years). These tumors typically exhibit slow growth, primarily in the thoracic region, often associated with dull pain without neurological deficits.

Radiologically, MRI can unveil several characteristic signs of nerve sheath tumors. Among these, the fascicular sign stands out as one of the most common findings, where fascicular bundles manifest as hypointense foci within the hyperintense area on T2-weighted images. Furthermore, well-defined heterogeneous hypointense signals on T1-weighted images are commonly observed [12]. Other notable signs include the "split-fat sign", "target sign", and "entry-exit nerve sign" [7]. The entry–exit nerve sign, when present, serves as a distinctive MRI indicator of schwannomas, presenting as a hyperintense signal adjacent to a fusiform mass, as observed on T2-weighted MRI sequences.

Histologically, they exhibit characteristic Antoni A and Antoni B areas. Antoni A areas are highly cellular, comprising compacted spindle-shaped cells, while Antoni B areas are highly vascularized, reticular in structure, and lack distinct architectural features. Another hallmark of schwannomas in immunohistochemical examination is diffuse S-100 protein expression [10].

Genetic studies play a pivotal role in enhancing the precision and speed of diagnosis. A diverse array of genetic mutations has been linked to schwannomas, with a recent international consensus on diagnosis and nomenclature further solidifying understanding in this area [19]. For instance, sporadic schwannomas often exhibit loss of heterozygosity on chromosome 22, particularly prevalent in vestibular schwannomas compared to spinal schwannomas [20]. Another group is NF2-related schwannomatosis, where tumorigenesis follows a two-hit model. The initial event involves the germline inactivation of NF2, located on chromosome 22q12.2, followed by the somatic inactivation of NF2 of the trans allele [19,20]. Additionally, other groups such as SMARCB1-related schwannomatosis and LZTR1-related schwannomatosis exist. The SMARCB1 gene is situated on the long arm of chromosome 22 at position 11.23 (denoted as 22q11.23) [21], while the LZTR1 gene is situated on the long arm of chromosome 22 at position 11.21 (22q11.21), approximately 3 megabases centromeric to SMARCB1 and 9 megabases centromeric to NF2 [22]. In relation to these entities, a hypothesis has been proposed suggesting three stages and four hits, wherein the dual inactivation of both SMARCB1 or LZTR1 alleles, combined with the dual inactivation of NF2 alleles, leads to tumor development [19,20,23]. Moreover, the promoter methylation of LATS1 and LATS2, which are downstream mediators of NF2 in the Hippo signaling pathway, is commonly observed in sporadic schwannomas [6].

In the presented case, we identified NF2 genetic mutation only. In addition, we detected variants of unknown significance by the FMI test after reclassification by the PGMC platform (Table 2). However, their impact is currently unknown. Hence, exploring their functional consequences on proteins through experimentation could be interesting, especially in the physiopathology of schwannomas. No specific genetic mutation associated with paraspinal schwannomas has ever been identified in the existing literature.

The differential diagnosis of paraspinal lesions encompasses a wide range of entities, from benign to aggressive (Table 3). Therapeutic approaches vary based on the nature of the lesion. These lesions are infrequently documented in the literature, often presenting with limited imaging and clinically unique characteristics, rendering diagnosis challenging based solely on clinical data [24,25].

Table 3. Differential diagnosis of neoplasms affecting paraspinal nervous structures. MMNST: malignant melanotic nerve sheath tumor. MPNST: malignant peripheral nerve sheath tumor. EMA: epithelial membrane antigen. IP: intraneural perineurioma. STP: soft-tissue perineurioma.

Type	Schwannoma Benign [26]	Lipoma Benign [27]	Cauda Equina Neuroendocrine Tumor (Ex- Paraganglioma) Benign [28]	Neurofibroma Benign [26]	Perineurioma Benign [26]	Hybrid Nerve Sheath Tumor Benign [29]	Malignant Peripheral Nerve Sheath Tumor (MPNST) Malignant [30]	Malignant Melanotic Nerve Sheath Tumor (MMNST) Malignant [31]
Common localization	Head and neck flexor surfaces of extremities; 70% intradural, 15% entirely extradural, 15% both intra- and extradural (dumbbell shape)	Most subcutaneous minority deeper locations	Lumbo-sacral region, solitary	Superficial locations (most lesions originate from small nerves)	IP: upper limbs and lower limbs. STP: superficial soft tissues of extremities and trunk	From most to least frequent, schwannoma/perineurioma occurs in extremities in form of subcutaneous/dermal masses	Sciatic nerve, brachial plexus, sacral plexus	Solitary outgrowth from spinal nerve roots and autonomic ganglia
Epidemiology	5% of all benign soft-tissue neoplasms. Mainly solitary lesions between 20 and 50 years of age	2% population	Male > female; no specific decade	5% of all benign soft-tissue neoplasms; young individuals 20–30 years of age	Two main types: 1-intraneural perineurioma (IP), more frequent in adolescents and young adults; 2-soft-tissue perineurioma (STP), more frequent in adults	Neurofibroma/schwannoma is overrepresented in patients with genetic syndrome (schwannomatosis, NFA, NF2) neurofibroma/perineurioma	Incidence per 10^6 people per year; 50–60% of MPNSTs occur in patients with NF1	Subset associated with Carney complex
Imaging characteristics (MRI) [32]	T1 iso/hypointense. T2 hyperintense. Well-circumscribed. Uniform to heterogeneous to peripheral enhancement. Size inferior to 5cm	T1 high signal, saturates on fat-saturated sequences, no or minimal enhancement. T2 high signal on FSET2	T1 hypo- to isointense. T2 iso- to hyperintense, characteristic "salt and pepper" appearance (rich vascular nature). T1 C+ homogeneous enhancement. Serpiginous flow void around tumor (dilated vessels or congested veins attributed to hypervascularity)	T1 hypointense. T2 iso/hyperintense. T2 fat-saturated hyperintense. T1 C+ heterogeneous enhancement Target sign: central low or intermediate signal intensity on T2-weighted images (fibrous tissue) surrounded by rim of higher signal intensity (myxoid tissue)	Fusiform enlargement of nerve with increased T2 signal and contrast enhancement	Very rare description in the literature	T2 hyperintense heterogeneous. T1 isointense to muscles. Peripheral contrast enhancement pattern. Irregular shape and indistinct margins. Large size (>5cm). Perilesional edema, intra-tumoral cystic changes. Low minimum ADC values	Well-circumscribed. T1 hyperintense. T2 hypointense (due to paramagnetic free radicals in melanin) [31]
Imaging characteristics (CT)	Isodense	Superficial circumscribed low attenuation mass	Vividly enhancing soft-tissue mass at level of the conus medullaris Rarely calcifies. If big enough, it can induce bony erosions of neighboring vertebrae	Well-defined hypodense mass. Minimal or no contrast enhancement	Hypodense relative to skeletal muscle		No CT findings which distinguish MPNST from neurofibroma	Isointense to hyperattenuating lesions. Possible calcifications. Bone remodeling and erosions are possible
Genetic	Loss of heterozygosity on chromosome 22 (sporadic schwannoma) NF2 (schwannomatosis)	Structural changes at 12q13-15. 13q and 6p21-23 regions	Rarely show loss of chromosome 3 (compared to pheochromocytomas and extra-adrenal paragangliomas)	Inactivation of NF1 gene (chromosome locus 17q11.2) encoding neurofibromin	IP: TRAF mutation. STP: no evidence of TRAF7 mutations	Schwannoma/perineurioma: usually sporadic neurofibroma/schwannoma associated usually with NF1, NF2, and schwannomatosis. Neurofibroma/perineurioma: associated usually with NF1	CDKN2A inactivation	Loss of function mutations in PRKAR1A (chromosome locus 17p22-24)
Immuno- histochemistry	PS100- and SOX10-positive (typically) CD57-positive antiKi67 1%	HMGA2-positive MDM2- CKD4-, p16-negative	Zellballen pattern in histology. PS100-positive. Keratin cocktail-positive. Chromogranin-positive. GATA3-negative. HOXB13-positive. Ki-67 low	PS100- and SOX10-positive. CD34-positive in stroma. EMA-positive in perineurial cells; antiKi67 1%	EMA-, Glut-1-, Claudin-1-positive (antigens in normal perineurium). PS100-negative. Mitotic activity low to absent	Schwan cells. PS100-positive. Perineural areas are positive for EMA, Glut-1. Neurofibromatous areas are positive for PS100, SOX10, EMA, and CD34	PPS100-positive in 50–70% cases; antiKi67 5–65%	PS100; SOX10 melan-1. HMB45-positive collagen IV tends to outline tumor lobules
Treatment	Surgery for gross total resection	Abstention; sometimes surgery (cosmetic, local pain)	Surgical gross total resection	Not associated with NF1 localized and diffuse lesion surgery but may require sacrifice of nerve. Associated with NF1: often non-surgical because of multiplicity of lesions (unless debilitating symptoms)	IP: no standard treatment guidelines but complete resection with nerve grafting. STP: complete excision (recurrences are uncommon)	Surgical gross total resection	Surgical ablation with wide resection margins. Responds poorly to chemotherapy and radiation	Surgical gross total resection

After compiling a comprehensive summary of the most common paraspinal lesions, we organized them into one table (Table 3), detailing their frequent localization, epidemiology, imaging characteristics (CT and MRI), genetic and immunohistochemistry features, and recommended treatments for each. Our analysis revealed that the localization of the lesions and their imaging characteristics on CT and MRI scans are not consistently specific. The majority of paraspinal lesions were isodense on CT scans and exhibited hypointensity on T1-weighted MRI images, along with hyperintensity on T2-weighted MRI images. However, immunohistochemistry, coupled with molecular studies, emerges as the most relevant approach for distinguishing between lesions and providing accurate diagnoses based on genetic variations and expressed antigens. Therefore, the utilization of appropriate histological and molecular criteria is imperative to refine diagnosis and determine the most effective treatment strategy [8]. Regarding treatment modalities, gross total resection is typically employed for nearly all lesions, with variations in the urgency of surgical intervention and the necessity for postoperative chemo/radiotherapy contingent upon the specific diagnosis. One of the most concerning entities is sarcomas, which are aggressive and highly proliferative neoplastic lesions requiring prompt diagnosis and treatment. Monitoring these lesions by imaging alone is inadequate, and complete surgical excision is essential.

5. Conclusions

Adopting a comprehensive approach is primordial in the management of paraspinal lesions. This involves gathering a detailed medical history, conducting a thorough physical examination, and performing laboratory analyses and radiological studies. However, given the broad differential diagnosis and the diagnostic uncertainty based solely on radiological findings, it is crucial to incorporate a systematic and reliable secure fine-needle biopsy as part of the preoperative investigation. Secure biopsy entails resecting soft tissues along the biopsy trajectory to mitigate the risk of dissemination in case of malignancy. Ideally, these biopsies should be conducted at specialized centers, where neurosurgeons collaborate closely with radiologists to accurately identify the target area. This collaboration should be followed by information exchange and group discussions with pathologists to enhance the accuracy of the pathology report.

Preoperative biopsies are indispensable in selecting the appropriate therapy, aiding surgeons in determining the optimal surgical technique, and reducing the risk of unnecessary complications and overtreatment. Once paraspinal schwannoma is diagnosed, the standard therapeutic approach is gross total resection, which is typically straightforward and associated with minimal complications. Despite the low risk (1%) of malignant transformation into neurofibrosarcoma, the risk–benefit ratio strongly supports complete surgical excision.

Furthermore, the risk of recurrence after a 12-month follow-up period is minimal, making postoperative chemotherapy or radiotherapy unnecessary. Although NF2 genetic mutations are well documented in NF2-related schwannomatosis, they have not been previously reported in paraspinal schwannomas. Our genetic and molecular analyses identified this mutation within paraspinal schwannomas in addition to several variants of unknown significance, highlighting the need for further exploration of their impact on protein production. This investigation is vital for advancing our understanding of the pathophysiology of schwannomas.

Author Contributions: H.S. and K.D. jointly conceived the study. H.S. and W.K. cared for the patient and carried out the operation and wrote the manuscript with R.K., A.M., A.P., M.D., E.C. and F.C. cared for the patient and drafted and revised the manuscript. All authors have read and agreed to the published version of the manuscript.

Funding: This research received no external funding.

Informed Consent Statement: The patient provided informed consent for inclusion prior to participating in the study, including agreement for a large-panel gene analysis on the extracted lesion, the subcontracting of the analysis, and the use of associated data.

Institutional Review Board Statement: The committee recommended informed consent of the patient only without realization of the ethical committee approval file, since the study dealt with surgical material already removed operatively without further intervening in the patient.

Data Availability Statement: The original contributions presented in this study are included in the article. Further inquiries can be directed to the corresponding author(s).

Conflicts of Interest: The authors have no conflicts of interest to declare.

References

1. Creze, M.; Ghaouche, J.; Missenard, G.; Lazure, T.; Cluzel, G.; Devilder, M.; Briand, S.; Soubeyrand, M.; Meyrignac, O.; Carlier, R.-Y.; et al. Understanding a mass in the paraspinal region: An anatomical approach. *Insights Imaging* **2023**, *14*, 128. [CrossRef]
2. Creze, M.; Soubeyrand, M.; Timoh, K.N.; Gagey, O. Organization of the fascia and aponeurosis in the lumbar paraspinal compartment. *Surg. Radiol. Anat.* **2018**, *40*, 1231–1242. [CrossRef]
3. Vasques, F.; Stecco, C.; Mitri, R.; De Caro, R.; Fusco, P.; Behr, A.U. Blocking around the *transversalis fascia*: Behind the scene. *Minerva Anestesiol.* **2019**, *85*, 15–20. [CrossRef]
4. Bond, J.D.; Zhang, M. Clinical Anatomy of the Extradural Neural Axis Compartment: A Literature Review. *World Neurosurg.* **2020**, *142*, 425–433. [CrossRef] [PubMed]
5. Stecco, C.; Tiengo, C.; Stecco, A.; Porzionato, A.; Macchi, V.; Stern, R.; De Caro, R. Fascia redefined: Anatomical features and technical relevance in fascial flap surgery. *Surg. Radiol. Anat.* **2013**, *35*, 369–376. [CrossRef]
6. Oh, J.-E.; Ohta, T.; Satomi, K.; Foll, M.; Durand, G.; McKay, J.; Le Calvez-Kelm, F.; Mittelbronn, M.; Brokinkel, B.; Paulus, W.; et al. Alterations in the NF2/LATS1/LATS2/YAP Pathway in Schwannomas. *J. Neuropathol. Exp. Neurol.* **2015**, *74*, 952–959. [CrossRef] [PubMed]
7. Valsecchi, D.; Galley, J.; Verzellotti, S.; Dontschev, A.; Mondragon, P.; Otten, P.; Maestretti, G. Paraspinal Intramuscular Schwannoma: Case Presentation and Literature Review of a Rare Pathology. *Open J. Mod. Neurosurg.* **2022**, *12*, 117–126. [CrossRef]
8. Ohla, V.; Scheiwe, C. A Purely Paraspinally Located Schwannoma from a Dorsal Root of a Spinal Nerve. *J. Adv. Med. Med. Res.* **2014**, *4*, 1366–1370. [CrossRef] [PubMed]
9. Kim, D.-G.; Jo, Y.-M. Paraspinal Ancient Schwannoma of the Dorsal Ramus Nerve: A Case Report. *J. Korean Soc. Spine Surg.* **2019**, *26*, 111–115. [CrossRef]
10. Kim, J.H.; Cho, T.G.; Kim, C.H.; Moon, J.G.; Lee, H.K. Erector Spinal Muscular Schwannoma of the Dorsal Ramus Nerve: A Case Report. *Korean J. Spine* **2015**, *12*, 204–206. [CrossRef] [PubMed]
11. Kim, Y.G.; Kim, T.W.; Kim, M.A.; Park, K.H. Schwannoma in the Dorsal Paraspinal Muscle: A Case Report. *Nerve* **2020**, *6*, 93–95. [CrossRef]
12. Shah, K.A.; Shah, A.C. Paraspinal Schwannoma of dorsal ramus nerve: A case report. *J. Clin. Orthop. Trauma* **2018**, *9*, S1–S4. [CrossRef]
13. Emengen, A.; Ergen, A.; Genç, M.H.; Kiraz, U.; İlbay, M.K. A cervical paravertebral schwannoma: A case report. *Med. Sci. Discov.* **2019**, *6*, 347–350. [CrossRef]
14. Keskin, H.; Kalkan, E.; Gündüz, E.; Ocak, G.A. An Uncommon Tumor: Paraspinal Schwannoma. *J. Cukurova Anesth. Surg. Sci.* **2020**, *1*, 28–33. [CrossRef]
15. Pace, S.; Sacks, M.A.; Minasian, T.; Hashmi, A.; Khan, F.A. Paraspinal plexiform schwannoma of unknown nerve origin: A case report. *Int. J. Surg. Case Rep.* **2021**, *79*, 267–270. [CrossRef] [PubMed]
16. Milbury, C.A.; Creeden, J.; Yip, W.-K.; Smith, D.L.; Pattani, V.; Maxwell, K.; Sawchyn, B.; Gjoerup, O.; Meng, W.; Skoletsky, J.; et al. Clinical and analytical validation of FoundationOne®CDx, a comprehensive genomic profiling assay for solid tumors. *PLoS ONE* **2022**, *17*, e0264138. [CrossRef]
17. Baux, D.; Van Goethem, C.; Ardouin, O.; Guignard, T.; Bergougnoux, A.; Koenig, M.; Roux, A.-F. MobiDetails: Online DNA variants interpretation. *Eur. J. Hum. Genet.* **2021**, *29*, 356–360. [CrossRef]
18. Agathe, J.-M.d.S.; Filser, M.; Isidor, B.; Besnard, T.; Gueguen, P.; Perrin, A.; Van Goethem, C.; Verebi, C.; Masingue, M.; Rendu, J.; et al. SpliceAI-visual: A free online tool to improve SpliceAI splicing variant interpretation. *Hum. Genom.* **2023**, *17*, 7. [CrossRef] [PubMed]
19. Plotkin, S.R.; Messiaen, L.; Legius, E.; Pancza, P.; Avery, R.A.; Blakeley, J.O.; Babovic-Vuksanovic, D.; Ferner, R.; Fisher, M.J.; Friedman, J.M.; et al. Updated diagnostic criteria and nomenclature for neurofibromatosis type 2 and schwannomatosis: An international consensus recommendation. *Genet. Med.* **2022**, *24*, 1967–1977. [CrossRef]
20. Bian, L.G.; Sun, Q.F.; Tirakotai, W.; Zhao, W.G.; Shen, J.K.; Luo, Q.Z.; Bertalanffy, H. Loss of heterozygosity on chromosome 22 in sporadic schwannoma and its relation to the proliferation of tumor cells. *Chin. Med. J.* **2005**, *118*, 1517–1524.
21. Kalimuthu, S.N.; Chetty, R. Gene of the month: *SMARCB1*. *J. Clin. Pathol.* **2016**, *69*, 484–489. [CrossRef] [PubMed]

22. Smith, M.J.; Isidor, B.; Beetz, C.; Williams, S.G.; Bhaskar, S.S.; Richer, W.; O'Sullivan, J.; Anderson, B.; Daly, S.B.; Urquhart, J.E.; et al. Mutations in *LZTR1* add to the complex heterogeneity of schwannomatosis. *Neurology* **2015**, *84*, 141–147. [CrossRef] [PubMed]
23. Paganini, I.; Capone, G.L.; Vitte, J.; Sestini, R.; Putignano, A.L.; Giovannini, M.; Papi, L. Double somatic SMARCB1 and NF2 mutations in sporadic spinal schwannoma. *J. Neuro-Oncol.* **2018**, *137*, 33–38. [CrossRef] [PubMed]
24. Ghani, A.; Ariff, A.; Romzi, A.; Sayuthi, S.; Hasnan, J.; Kaur, G.; Awang, S.; Zamzuri, I.; Ghazali, M.; Abdullah, J. Giant nerve sheath tumour: Report of six cases. *Clin. Neurol. Neurosurg.* **2005**, *107*, 318–324. [CrossRef]
25. Page, M.J.; McKenzie, J.E.; Bossuyt, P.M.; Boutron, I.; Hoffmann, T.C.; Mulrow, C.D.; Shamseer, L.; Tetzlaff, J.M.; Akl, E.A.; Brennan, S.E.; et al. The PRISMA 2020 Statement: An Updated Guideline for Reporting Systematic Reviews. *BMJ* **2021**, *372*, n71. [CrossRef]
26. Belakhoua, S.M.; Rodriguez, F.J. Diagnostic Pathology of Tumors of Peripheral Nerve. *Neurosurgery* **2021**, *88*, 443–456. [CrossRef] [PubMed]
27. Thway, K.; Flora, R.; Shah, C.; Olmos, D.; Fisher, C. Diagnostic Utility of p16, CDK4, and MDM2 as an Immunohistochemical Panel in Distinguishing Well-differentiated and Dedifferentiated Liposarcomas From Other Adipocytic Tumors. *Am. J. Surg. Pathol.* **2012**, *36*, 462–469. [CrossRef]
28. Schweizer, L.; Thierfelder, F.; Thomas, C.; Soschinski, P.; Suwala, A.; Stichel, D.; Wefers, A.K.; Wessels, L.; Misch, M.; Kim, H.-Y.; et al. Molecular characterization of CNS paragangliomas identifies cauda equina paragangliomas as a distinct tumor entity. *Acta Neuropathol.* **2020**, *140*, 893–906. [CrossRef]
29. Lang, S.-S.; Zager, E.L.; Coyne, T.M.; Nangunoori, R.; Kneeland, J.B.; Nathanson, K.L. Hybrid peripheral nerve sheath tumor: Case report. *J. Neurosurg.* **2012**, *117*, 897–901. [CrossRef]
30. Coulon, A.; Milin, S.; Laban, E.; Debiais, C.; Jamet, C.; Goujon, J.-M. Aspects histopathologiques des principales tumeurs des nerfs périphériques. *Neurochirurgie* **2009**, *55*, 454–458. [CrossRef]
31. Hoover, J.M.; Bledsoe, J.M.; Giannini, C.; Krauss, W.E. Intramedullary Melanotic Schwannoma. *Rare Tumors* **2012**, *4*, e3. [CrossRef] [PubMed]
32. Fisher, S.; Karri, S.; Ramzi, A.; Sharma, R.; Chhabra, A.; Soldatos, T. Advanced MR Imaging of Peripheral Nerve Sheath Tumors Including Diffusion Imaging. *Semin. Musculoskelet. Radiol.* **2015**, *19*, 179–190. [CrossRef]

Disclaimer/Publisher's Note: The statements, opinions and data contained in all publications are solely those of the individual author(s) and contributor(s) and not of MDPI and/or the editor(s). MDPI and/or the editor(s) disclaim responsibility for any injury to people or property resulting from any ideas, methods, instructions or products referred to in the content.